Nonlinear-optical processes in the near-resonant two-photon excitation of xenon by femtosecond KrF-excimer-laser pulses

A. Tünnermann, K. Mossavi, and B. Wellegehausen
Institut für Quantenoptik, Universität Hannover, Welfengarten 1, 3000 Hannover 1, Germany
(Received 14 February 1992)

The nonlinear response of xenon gas due to a near-resonant two-photon excitation at the $5p^6\,{}^1S_0 \rightarrow 6p[\frac{1}{2}]_0$ transition with a femtosecond KrF-excimer-laser system is investigated for the intensity range 10^{10}–10^{15} W/cm^2. Stimulated hyper-Raman scattering and amplified spontaneous emission of atomic xenon are observed at wavelengths around 823 and 828 nm. These emissions are superimposed by four-wave parametric-oscillation processes leading to strong ultrashort continuum radiation in the visible and near-infrared (650–850 nm), uv (185–400 nm), and vacuum ultraviolet (147–155 nm) spectral ranges with output powers up to 100 MW. From difference-frequency-mixing experiments microscopic nonlinear susceptibilities in the range of $|\chi^{(3)}| = 10^{-48}$ to 10^{-50} m^5/V^2 have been determined, which are in good agreement with calculations.

PACS number(s): 32.80.Wr, 42.55.−f, 42.65.Ky, 42.65.Hw

I. INTRODUCTION

In the interaction of intense radiation fields with matter, multiphoton excitation and ionization processes occur. Basic investigations and reviews about these processes are given in Refs. [1–3]. Also the nonlinear response of the medium is the subject of studies and research [4,5] and is applied for the generation or radiation at shorter wavelengths [6–8]. If the pump laser is operated near or at an allowed two-photon transition, multiphoton-absorption and -ionization processes are resonantly enhanced. In combination with multiphoton absorption, other phenomena such as amplified spontaneous emission (ASE), stimulated hyper-Raman scattering (SHRS) [3], and four- or six-wave-mixing processes (FWM, SWM), driven by ASE, SHRS, or additional external pump laser fields can be observed [9,10].

The generation of coherent tunable vacuum ultraviolet (vuv) radiation by frequency mixing is an established technique for nanosecond pump-laser pulses. The most commonly used techniques are difference and sum frequency mixing or frequency tripling in gases and vapors. Metal vapors [11–13] as well as noble gases [14–16] are suited as nonlinear media. FWM has also been observed in molecular gases and vapors [17,18]. In these four-wave-mixing schemes three pump fields are applied to generate a fourth short-wavelength coherent field. For nonresonant mixing processes conversion efficiencies typically in the range of 10^{-5}–10^{-7} have been realized, whereas for the two-photon resonantly enhanced mixing schemes efficiencies up to 1% have been measured.

Recently FWM processes in atomic and molecular gases have also been observed by applying only two pump-laser fields, in general of the same frequency [18–21]. In these parametric four-wave-mixing or four-wave parametric-oscillation schemes (PFWM, FWPO), two coherent fields are generated simultaneously from quantum noise, comparable to the optical parametric oscillation (OPO) in solids [22,23]. The generated frequencies are determined by the energy conservation law and the phase-matching condition $\Delta k = 0$.

In this paper we report the observation of ASE, SHRS, FWPO, and FWM in xenon pumped by a femtosecond KrF-excimer-laser system. The observed nonlinear processes are due to a near-resonant two-photon excitation of the xenon $6p$ states by the 248.5-nm pump-laser radiation (Fig. 1). ASE is detected on $6p \rightarrow 6s$ transitions at 823 and 828 nm, broadened by SHRS. The oscillations occur in forward and also in backward direction with respect to the pump laser. In addition to these emissions, intense continua in the visible, uv, and vuv spectral range

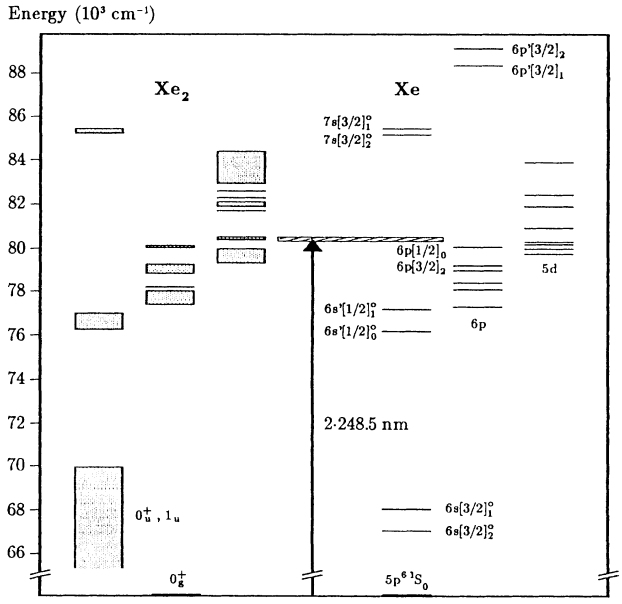

FIG. 1. Relevant energy-level diagram of atomic and molecular xenon. Molecular absorption bands are indicated by the hatched areas (after Refs. [24,25]).

are observed, which correspond to FWPO and secondary FWM. These processes are noncollinear phase matched; no anomalous dispersion is required for optimum conversion. In the experiments output powers up to 100 MW and spectral widths exceeding 4000 cm^{-1} have been measured [26]. Similar emission characteristics but at less output intensity, to our knowledge, have only been obtained so far in connection with the generation of super continuum radiation in the interaction of ultrashort pulses with solids, liquids, and high-pressure gases [27].

The dependence of generated coherent emissions on xenon pressure in the intensity range $10^{10}-10^{15}$ W/cm^2 is studied. For the investigated FWM schemes conversion efficiencies up to several percent have been measured. Due to the high peak intensities of the KrF-pump-laser system, a resonant enhancement of the SHRS and the four-wave-mixing processes has been observed, as the $6p$ states are shifted into the two-photon resonance by the ponderomotive potential. Experimental results are discussed and compared with theoretical estimations.

II. EXPERIMENT

For the experiments a femtosecond KrF-excimer-laser system, described in detail in Ref. [28], was used, yielding 10 mJ in 360 fs at a fixed wavelength of 248.5 nm. The pulse duration of the linear polarized pump laser was controlled by an autocorrelator based on two-photon ionization of NO [29] and on-line by a single-shot autocorrelator using a two-photon ionization process in cadmium [30]. In the focused beam intensities up to 10^{15} W/cm^2 (spot size: $\Phi=50$ μm; confocal parameter: $z_k=16$ mm) are reached. By dielectric attenuators the pump-laser radiation could be diminished continuously. The spectral bandwidth of the KrF-pump-laser pulse is about $\Delta\nu\approx 100$ cm^{-1} (bandwidth product: 1.23; Fourier-limit $sech^2$ pulse: 0.31).

The radiation of this laser system was focused by an $f=1000$ mm lens into a cell filled with xenon gas. The cell was equipped with LiF windows and has been operated at gas pressures between 0.05 and 760 Torr. The generated radiation was investigated parallel (forward), antiparallel (backward), and transversal to the pump-laser direction. The radiation emitted in the direction of the pump-laser beam was collimated by an $f=300$ mm LiF lens. The transversally emitted fluorescence could be observed by windows in the focus region of the pump laser. The spectral range $\lambda=115-1200$ nm was examined by different monochromators in connection with multipliers (CsJ, multi-alkaline-earth, and $S1$ characteristic). Spectra were taken by a boxcar averager, controlled by a computer system. The temporal characteristics were studied by a transient digitizer ($\Delta t>0.8$ ns) or in the visible and uv spectral range by a streak camera and Michelson-type autocorrelators. In order to cover different spectral ranges, the autocorrelator was equipped with frequency doubling crystals or an ionization chamber as nonlinearity. The purity of the gases used was on the order of 99.99%. The optical pathways outside the xenon cell could be evacuated to less than 10^{-3} Torr, in order to prevent an absorption of the generated vuv radiation. Output energies in all investigated wavelength ranges were measured by calibrated pyroelectric power meters. The beam profile of the emitted radiation could be examined by a charge-coupled-device (CCD) camera system.

III. RESULTS AND DISCUSSION

By irradiating the xenon cell with the fs KrF-excimer-laser pulse, a variety of distinct coherent emissions in different spectral ranges are observed. Depending on the xenon pressure, the radiation consists of atomic line oscillation in the near infrared at wavelengths of 828 and 823 nm, an intense continuum in the uv around 280 nm, and a broadband emission between 650 and 850 nm in correlation with vuv radiation around 148 nm.

The line oscillation was found to result from ASE and SHRS. Experiments on this process are described and discussed in Sec. III A. In Sec. III B investigations on the continuum emissions, which are due to FWPO and FWM processes are presented and analyzed.

A. Amplified spontaneous emission and stimulated hyper-Raman scattering in the atomic xenon

Upon the excitation of the xenon gas with the fs KrF-excimer-laser system a strong fluorescence transversal to the pump-laser direction is obtained in the near-infrared spectral range [Fig. 2(a)]. At a pump-laser energy of about 6 mJ ($I>10^{14}$ W/cm^2) the emission consists of five atomic lines that can clearly be attributed to the xenon $6p\rightarrow 6s$ transitions. The intensity of the 823- and 828-nm fluorescence line corresponds well to the oscillator strengths of the transitions [31], indicating a direct population of the upper levels with the same excitation rate. These strong fluorescences can only be observed at high intensities, due to the small two-photon absorption cross sections of the pump-laser radiation at the given detunings ΔE from the resonances (two-photon absorption cross sections around 10^{-36} cm^4/W have been measured [32]). Because of the high peak intensities of the pump-laser system, it has also to be assumed that the levels are shifted transient into the two-photon resonance, resulting in an enhancement of the excitation rates (see below).

On two of the $6p\rightarrow 6s$ transitions, the $6p[\frac{1}{2}]_0\rightarrow 6s[\frac{3}{2}]_1^o$ transition ($\lambda=828$ nm, $\Delta E=363$ cm^{-1}) and the $6p[\frac{3}{2}]_2\rightarrow 6s[\frac{3}{2}]_2^o$ transition ($\lambda=823$ nm, $\Delta E=1270$ cm^{-1}), stimulated emission parallel [Fig. 2(b)] and also antiparallel [Fig. 2(c)] to the pump-laser direction occurs. In these laser spectra the intensity ratio is reversed in comparison to the fluorescence spectrum. This is due to the disadvantageous degeneration factors of the upper and lower laser levels for the 823-nm transition compared to the 828-nm transition, leading to a strong reduction of the inversion density. In addition, the $6s[\frac{3}{2}]_2^o$ state is not dipole coupled to the xenon ground state, which results—because of the metastability of this lower laser level—in a self-terminating laser scheme. The output energy of the two laser transitions was found to increase first nearly exponential with the pump power, but then starts to saturate at a pump energy above 2 mJ. The

pressure dependence for the emission is given in Fig. 3. A slight saturation can be observed for xenon pressures above 200 Torr. At the maximum used xenon pressure of 760 Torr and for optimum pump-laser energies of 6.5 mJ, output energies of about 45 μJ are detected in forward direction, whereas in backward direction the output intensity was less by a factor of more than 50, which is typical for short pulse traveling-wave excitation schemes. The temporal characteristics of these emissions have been studied by a streak camera. No significant delay of the infrared emission with respect to the excitation pulse could be observed. A typical pulse shape is shown in Fig. 4. The pulse duration was found to be about 70 ps, which is much larger than the pump-laser pulse and indicates again that a population transfer process into the $6p$ levels

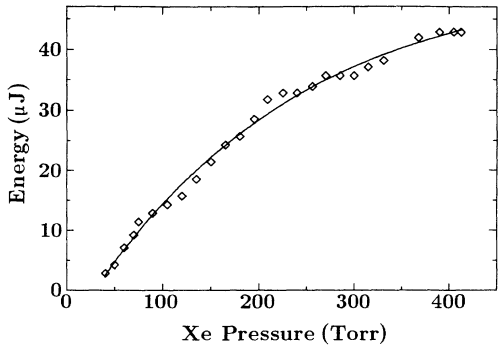

FIG. 3. Output energy at $\lambda=828$ nm vs xenon pressure. Pump-laser energy: 5 mJ.

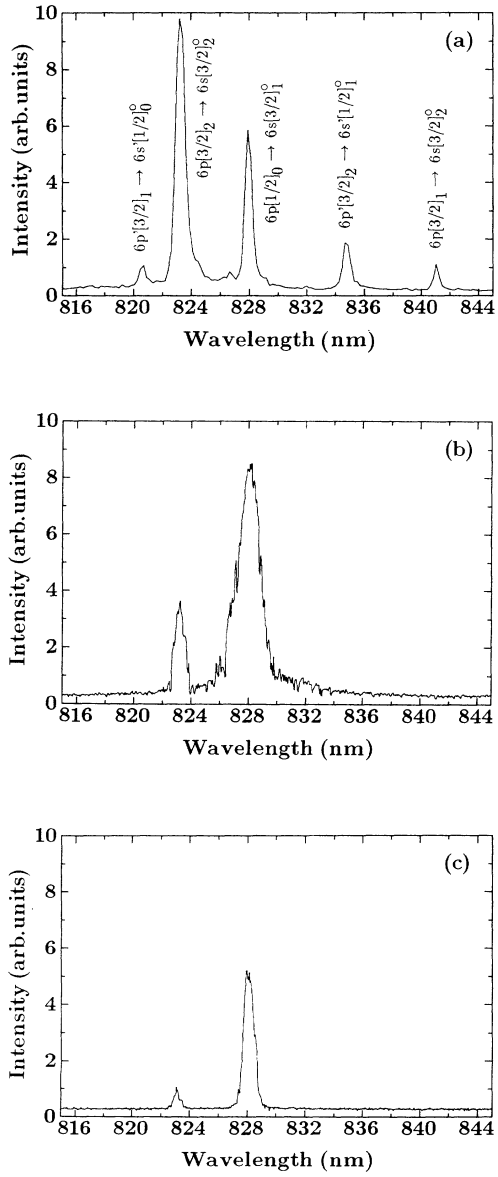

FIG. 2. Near-infrared emission spectra of atomic xenon at a gas pressure of 150 Torr and a pump-laser energy of 6 mJ. (a) Transversal; (b) parallel; (c) antiparallel.

occurs, resulting in amplified spontaneous emission at the $6p \rightarrow 6s$ transitions.

The spectral width of the forward and backward emissions at 828 and 823 nm strongly increases symmetrically around the atomic resonances with the xenon pressure as shown in Fig. 5, in contrast to the transversal fluorescence. At xenon pressures above 700 Torr the spectral width exceeds 50 cm^{-1} and becomes comparable to the bandwidth of the pump-laser system. At these pressures the two laser lines overlap. In addition, the degree of linear polarization, corresponding to the pump-laser polarization, increases from almost zero at lower pressure to more than 40% at xenon pressures above 500 Torr. The polarized emission contribution occurs like the ASE oscillation coaxial to the pump-laser beam (parallel and antiparallel to the pump-laser direction) and behaves almost identically on both laser transitions. To explain the broadening of the emissions and the increase of linear polarization, we assume that an increasing amount of SHRS parallel and antiparallel to the pump-laser direction is added to the ASE emission on both transitions (Fig. 6). For the 828-nm emission no reduction of the SHRS is obtained, although the lower $6s[\frac{3}{2}]^{\circ}_{1}$ level is dipole coupled to the xenon $5p$ ground state, which should lead to a suppression of SHRS as has been observed in nanosecond pump-laser experiments [19,21,33]. The suppression in these experiments was due to interference effects between the polarization induced by the pump laser and the generated hyper-Raman pulse, an effect which could not be

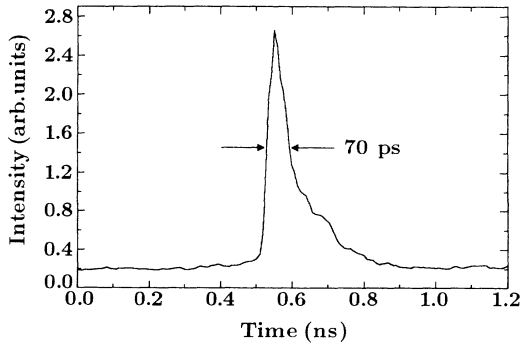

FIG. 4. Streak camera recording of the parallel infrared line emission at $\lambda=828$ nm.

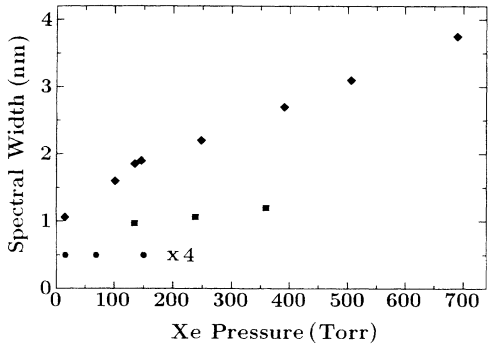

FIG. 5. Spectral width of the $\lambda=828$ nm emission for increasing xenon pressure. ●: Transversal; ■: antiparallel; ◆: parallel.

observed in our experiments, probably because of the fast transients in the examined system and group velocity dispersion effects.

In addition, no indications for contributions from four-wave-mixing processes have been found. Such processes can be excluded for this collinear emission because the necessary phase-matching condition $\Delta k=0$ can only be satisfied for a collinear emission in a regime of anomal dispersion above the 6*s* levels, whereas here the transitions are broadened symmetrically around the atomic resonances. In addition, no coherent emissions in the corresponding vuv spectral range have been observed.

A hyper-Raman pulse should be emitted in a time scale corresponding to the pulse duration of the pump laser. However, we cannot yet observe such a short pulse component within the strong picosecond ASE emission (see also Fig. 4), but regarding the spectral bandwidth of the emission, fs-pulse components should be possible. For a clear separation of ASE and SHRS, experiments with tunable pump-laser radiation would be necessary.

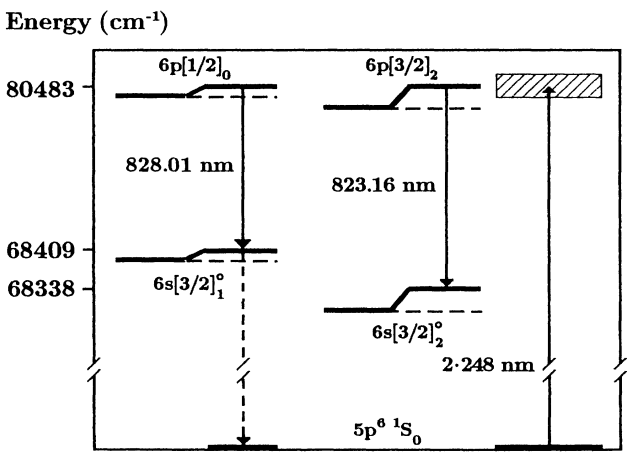

FIG. 6. Observed laser transitions in the atomic xenon. The hatched area indicates the spectral width of the pump laser. The energy shift of the involved levels according to the ponderomotive potential is also shown.

In the experiments a population of the $6p[\frac{1}{2}]_0$ and the $6p[\frac{3}{2}]_2$ levels is observed, leading to fluorescence, ASE, and near-resonant hyper-Raman emission. The transversal fluorescence of the 6*p* levels [see also Fig. 2(a)] depends quadratically on the pump-laser energy as can be seen from Fig. 7, indicating a two-photon excitation process.

In the experiments the emissions occur at resonance, although the pump laser is detuned from the two-photon resonance by about 363 and 1270 cm^{-1}, respectively. Therefore the energy detunings for the assumed hyper-Raman emission must be neutralized during the interaction process. An intensity-dependent process must shift the 6*p* levels and also the 6*s*, because the emission wavelengths of the two transitions at 828 and 823 nm are not changed in this process. Such a behavior is observed in above-threshold-ionization (ATI) experiments by Shakeshaft and co-workers [4], where energetically high-lying states are shifted by the ponderomotive potential U_p [34,35]. In the approximation of loosely bound electrons the energy shift U_p of the upper and lower laser levels, corresponding to this pondermotive potential in the case of the xenon atom (reduced mass μ), for different pump-laser intensities (I) at the KrF-laser wavelength ($\lambda=2\pi c/\omega$) can be calculated from

$$U_p=\frac{e^2I}{2\epsilon_0\mu\omega^2c}\ , \tag{1}$$

where ϵ_0 is the dielectric constant, e the elementary charge, and c the velocity of light. For the neutralization of the energy detuning of the 6*p* states (see also Fig. 6) a pump-laser intensity of 8×10^{12} W/cm^2 ($\Delta E=363$ cm^{-1}) and 3×10^{13} W/cm^2 ($\Delta E=1270$ cm^{-1}), respectively, is necessary, if the energy shift of the electronic states is mainly determined by the shift of free electrons. From these values it can be concluded that with increasing pump-laser intensity an emission out of the $6p[\frac{1}{2}]_0$ state should be detected first, whereas an emission out of the $6p[\frac{3}{2}]_2$ level should occur at a much higher intensity. This behavior can be observed when the dependence of the ratio of the output intensity for the 823- and 828-nm laser transitions on the pump-laser energy (Fig. 8) is examined. For pump-laser energies in the range of 0.1 mJ

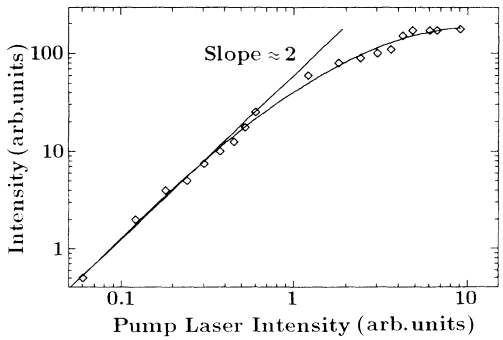

FIG. 7. Log-log plot of the transversal fluorescence intensity ($\lambda=828$ nm) vs pump-laser intensity.

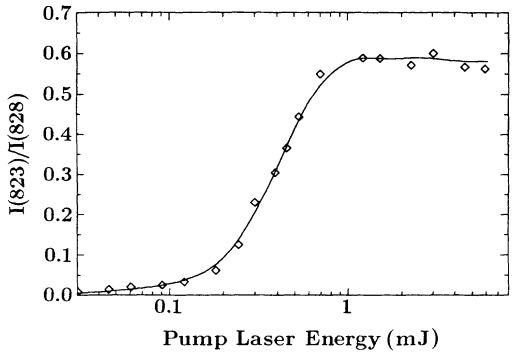

FIG. 8. Ratio of the output intensity for the 823- and 828-nm laser transitions vs pump-laser energy.

($I < 10^{13}$ W/cm^2) the xenon laser spectrum is dominated by the 828-nm laser transition, whereas the 823-nm transition only occurs when higher pump energies are used, resulting in stronger level shifts. At still higher pump-laser intensities, which are correlated with larger energy detunings, both levels are populated further on, because of the transient following of the ponderomotive potential with the femtosecond-pulse shape. This process might be superimposed by a larger pump intensity threshold at the 823-nm transition compared to the intensity necessary at 828 nm as discussed recently by Davis and Dressler [36] in a resonant two-photon excitation for pump pulse durations of several hundred ps, and additional saturation effects which can also lead to a broadening of the spectra.

B. Four-wave parametric oscillation and four-wave mixing

In addition to the infrared line oscillation three strong coherent continuum emissions in the visible and near-infrared (650–850 nm), in the uv (185–400 nm), and in the vuv (147–155 nm) spectral ranges are observed. Thereby, the visible and vuv emissions are strongly correlated and are emitted as the uv emission in a four-wave parametric-oscillation process. Both processes are optimum in different xenon pressure ranges.

1. Visible and vuv emission

Figure 9 gives spectra in the range 650–860 nm, parallel, antiparallel, and perpendicular to the pump-laser beam. The forward emission [Fig. 9(a)] is centered at about 760 nm with a spectral bandwidth of nearly 100 nm at a xenon pressure around 80 Torr. With increasing xenon pressure the center wavelength is slightly shifted to shorter wavelengths. Superimposed on this broadband signal the two infrared lines at 823 and 828 nm, discussed above, can be seen. In backward direction [Fig. 9(b)], collinear to the pump laser, a similar continuum is emitted, however, at a much smaller bandwidth and at an intensity typically by a factor of more than 1000 less. The fluorescence signal detected transversal to the pump laser [Fig. 9(c)] is quite different from the forward and backward signals. On a broad background, resulting from xenon molecules as discussed below, a variety of atomic and ionic xenon lines can be seen, as a result of multiphoton ionization followed by relaxation and recombination processes. The strong coherent forward emission has been further optimized to increase the output energy and analyzed with respect to its temporal and spatial structure.

The dependence of the spectral integrated output energy on the pump-laser energy (Fig. 10) and the xenon pressure (Fig. 11) has been measured by pyroelectric energy meters. For these measurements the infrared line oscillation has been cut off by dielectric filters. An optimum output energy was achieved for a xenon pressure of 45 Torr and a pump-laser energy of about 5 mJ. The saturation and finally the decrease of the output energy with the

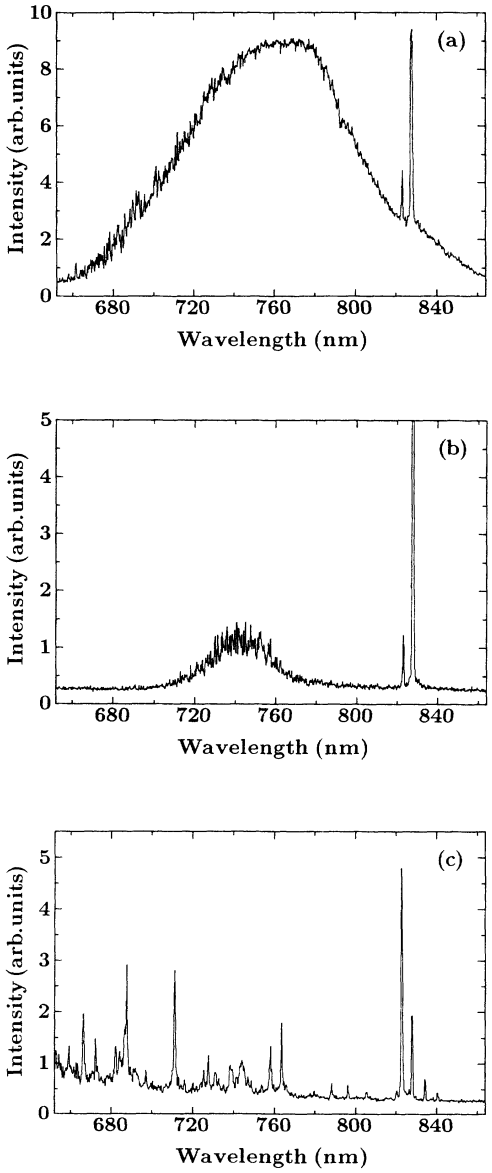

FIG. 9. Emission spectra in the wavelength range between 650 and 860 nm. Xenon pressure: 80 Torr; pump-laser energy: 5 mJ. (a) Parallel: coherent continuum emission. The infrared stimulated line emission is superimposed; (b) antiparallel; (c) transversal.

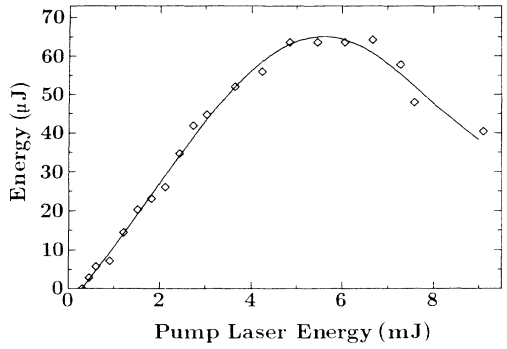

FIG. 10. Output energy of the visible continuum emission vs pump-laser energy; xenon pressure: 45 Torr.

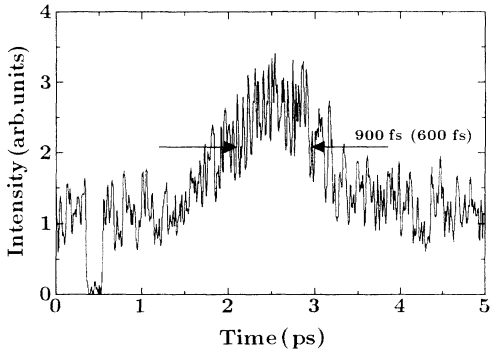

FIG. 12. Autocorrelation trace of the visible emission. Center wavelength 740±10 nm.

pump-laser energy is probably due to a multiphoton ionization of the xenon atoms, indicated by the production of electrons and ions in the interaction volume. For optimum conditions output energies of about 60 μJ have been detected. This value corresponds to a conversion efficiency of more than 1% of the pump-laser energy. The pulse duration of this radiation has been determined by measurements with a Michelson-type autocorrelator equipped with a potassium dihydrogen phosphate (KDP) crystal, which is phase matched by angle tuning. For these measurements the spectra width of the continuum radiation was reduced to about 20 nm by interference filters. A typical autocorrelation trace is shown in Fig. 12. From this curve a pulse duration of 600 fs can be determined for a sech^2 pulse. Taking into account the group velocity dispersion by the optical components in the laser beam, this pulse duration corresponds to the pump-laser pulse width of about 360 fs. The peak power for the continuum radiation therefore exceeds 100 MW.

The continuum emission is polarized according to the pump-laser polarization, indicating that in contrast to the infrared line emission no population transfer process occurs in the interaction. The most striking feature of this broadband visible emission in the forward direction is a conical emission profile as shown in Fig. 13. The cones have been recorded by a CCD camera system. For these measurements the spectral bandwidth of the continuum emission was reduced by interference filters. The diameter of the cones increases slightly with the emission wavelengths [Figs. 13(a) and 13(b)] and for a fixed wavelength with the xenon pressure [Figs. 13(c)–13(f)]. For a wavelength of 760 nm and a xenon pressure of 45 Torr an opening angle for the cone up to 5.2° has been measured, from which a walk-off distance can be estimated. This distance is defined as the length over which the pump-

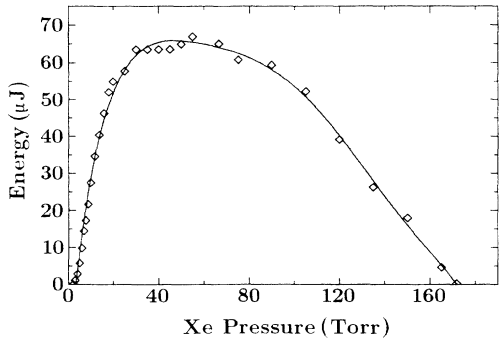

FIG. 11. Output energy of the visible continuum emission vs xenon gas pressure; pump-laser energy: 5mJ.

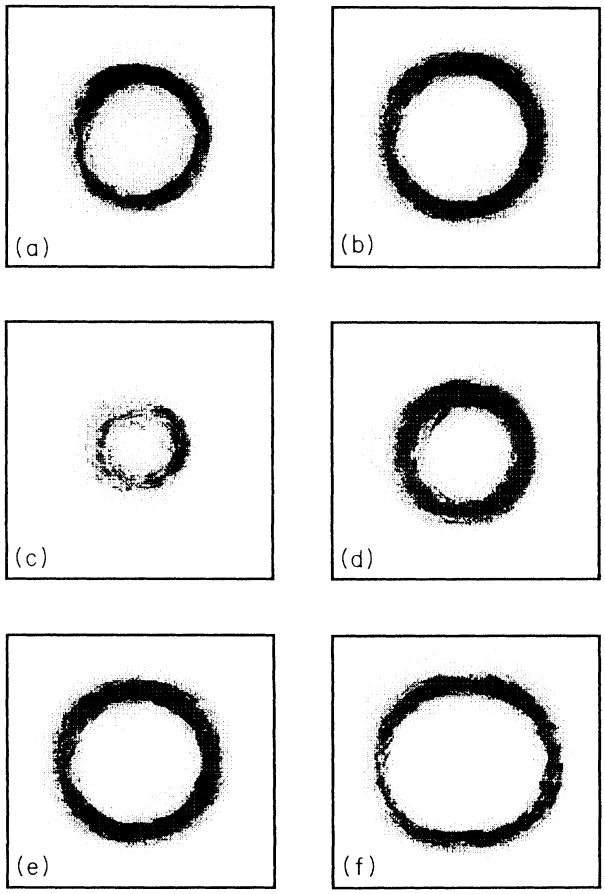

FIG. 13. Conical emission profiles of the visible radiation (forward direction) (a) $\lambda=670$ nm; (b) $\lambda=760$ nm; (c)–(f) increasing xenon pressure ($\lambda=760$ nm).

laser beam and the conically propagating beams generated in the interaction volume still overlap. For a cone half angle of 2.6° and a laser beam size of 50 μm the walk-off distance and therefore the interaction length between the KrF-pump laser and the generated radiation is only about 1.2 mm. As the cone angle increases in general with xenon pressure, this interaction length is further reduced at higher pressures. This leads to the reduction of the output energy with increasing xenon density as observed in the experiments (see also Fig. 11).

Correlated with the visible continuum emission, a coherent emission in the vuv at about 150 nm is observed parallel to the pump-laser direction [Fig. 14(a)]. A noticeable backward emission could not be detected. Also the transversal radiation is weak but shows a distinct structure between 150 and 170 nm [Fig. 14(b)]. This emission cannot result from the xenon atoms, because the longest-wavelength xenon resonance line is centered at about 146.9 nm. This transversal vuv emission is, as discussed below, of molecular origin.

The forward coherent emission is obtained between 147 and 153 nm and has a spectral width of about 2 nm [Fig. 14(a)]. By a variation of the xenon pressure in the range between 10 and 130 Torr the center wavelength of this emission can be shifted by about 4 nm from 148 to 153 nm with a slight spectral broadening. An optimum output energy of more than 30 μJ was obtained for a pressure of about 40 Torr (center wavelength: 148 nm) and a pump-laser energy of 5 mJ [Fig. 15]. At higher pump-laser energies a saturation of the emitted intensity

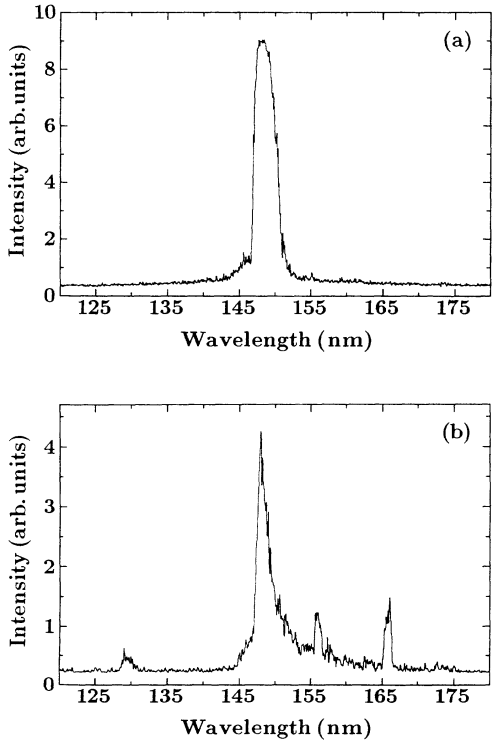

FIG. 14. Spectra of the vuv emission for a xenon pressure of 30 Torr and a pump-laser energy of 5 mJ. (a) Parallel; (b) transversal.

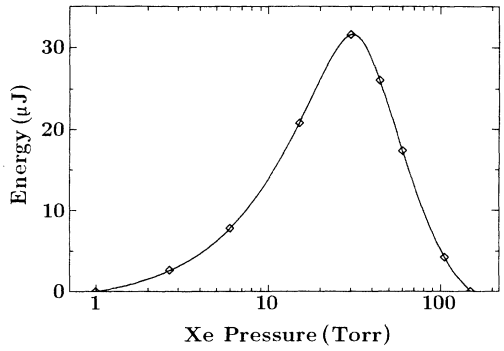

FIG. 15. Dependence of the generated vuv emission in forward direction on the xenon pressure; pump-laser energy : 5 mJ.

is obtained in the same way as that for the visible continuum emission. Regarding the dispersion of xenon near the 147-nm resonance, a slight pulse broadening of the vuv emission due to group velocity dispersion has to be assumed. In a Samson ionization chamber [37] the pulse duration of the vuv emission has been estimated by a two-photon ionization process in argon to be on the order of 10 ps, resulting in output powers of several megawatts.

The visible and the vuv emission show a comparable bandwidth of about 4000 cm^{-1} and a very similar behavior with respect to pressure and pump power dependence, polarization, and pulse duration, which all suggests a common generation process. Considering further that the sum of the center wave-lengths' photon energies of the correlated emissions corresponds to the energy of two pump-laser photons and that the shift of the center frequencies with pressure are opposite, keeping the sum constant, we come to the conclusion that the emissions are due to a parametric four-wave-mixing process:

$$2\omega_p = \omega_{\text{vis}} + \omega_{\text{vuv}} , \tag{2}$$

with ω_p, ω_{vis}, and ω_{vuv} being the frequencies of the pump, visible, and vuv emissions, respectively. For such a process a phase-matching condition

$$\Delta\mathbf{k} = 2\mathbf{k}_p - \mathbf{k}_{\text{vis}} - \mathbf{k}_{\text{vuv}} = \mathbf{0} \tag{3}$$

is necessary for the corresponding wave vectors $\mathbf{k}$. As the visible emission is emitted into a cone, a noncollinear phase matching as indicated in Fig. 16 has to be assumed. In the approximation of only a slightly depopulated

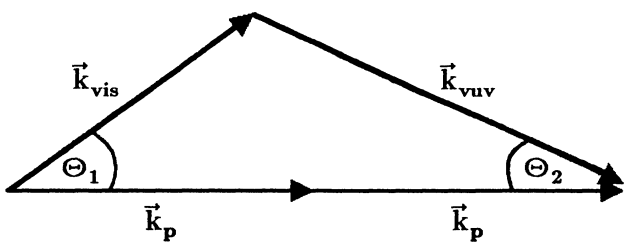

FIG. 16. Wave-number vector diagram for noncollinear phase matching.

ground state, the refraction index of the xenon gas can be determined by the Sell-maier equation [38,39]. Using this refraction index, the opening angles can be determined for the assumed noncollinear phase matching. As indicated in Fig. 17, the experimentally observed cone half angles for different xenon pressures, here at $\lambda=670$ nm represented by the rhombs, fit well to the theoretically determined dependence. The corresponding angles for the vuv emission are very small and cannot be measured yet. The small deviation of the experimental values compared to the theoretical values might be explained by higher-order nonlinear processes as multiphoton excitation and ionization, which modify the refraction index of the xenon gas. In addition, the refraction index is also influenced by the increasing number of xenon molecules with xenon pressure.

Different buffer gases have been added in order to modify the index matching and to realize a more collinear phase-matched four-wave-mixing scheme. However, no significant change of the output characteristics has been observed.

Considering the efficient simultaneous generation of the two continua and the absence of any strong input field at either $\omega_{\rm vis}$ or $\omega_{\rm vuv}$, we have to assume that the coherent radiation at $\omega_{\rm vis}$ and $\omega_{\rm vuv}$ is generated in a four-wave parametric-oscillation process, which corresponds to the optical parametric-oscillation process in solids. The waves $\omega_{\rm vis}$ and $\omega_{\rm vuv}$ build up from quantum noise by exponential amplification according to [22,40]

$$I_i = I_i(0)(G_0 l/2)^2 \frac{\sinh^2(Gl/2)}{(Gl/2)^2} \exp(-\sigma N L) , \quad (4)$$

with an amplification coefficient $G^2 = G_0^2 - (\Delta k)^2$ for a wave-vector mismatch Δk. I_i stands for the intensity of the generated fields at ω_i ($\omega_i = \omega_{\rm vis}$ or $\omega_{\rm vuv}$). The maximum amplification coefficient G_0 for optimum phase matching ($\Delta k = 0$) is given by [3,18,40]

$$G_0^2 = \frac{9\omega_{\rm vis}\omega_{\rm vuv}}{(2c^2\epsilon_0)^2 n_{\rm vis} n_{\rm vuv} n_p^2} |\chi^{(3)}|^2 N^2 I_p^2 , \quad (5)$$

with $\chi^{(3)}$ being the nonlinear microscopic susceptibility for the corresponding difference-frequency-mixing process [40], N the xenon density, and I_p the pump-laser intensity. $n_{\rm vis}$, $n_{\rm vuv}$, and n_p are the refraction indices of the waves with frequency $\omega_{\rm vis}$, $\omega_{\rm vuv}$, and n_p are the refraction indices of the waves with frequency $\omega_{\rm vis}$, $\omega_{\rm vuv}$, and ω_p, respectively. (All values are given in *Système International* units.)

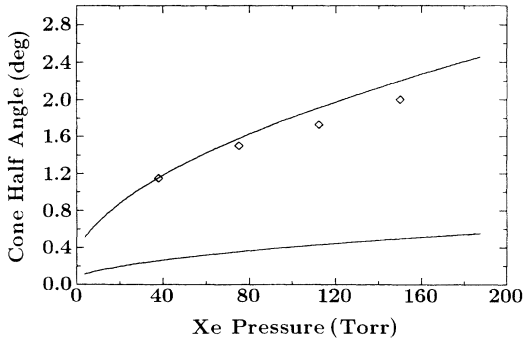

FIG. 17. Calculated cone half angles for different xenon pressures. Upper curve: $\lambda=670$ nm (Θ_1); lower curve: $\lambda=152$ nm (Θ_2); rhombs: experimental values.

In formula (4) l is an effective amplification length determined by the noncollinear phase-matching geometry and $I_i(0)$ is the intensity of the starting noise field. The factor $\exp(-\sigma NL)$ describes an additional absorption (cross section σ).

For $\Delta k = 0$ and assuming a high amplification and no absorption, formula (4) simplifies to a pure exponential increase of the intensity according to

$$I_i(l) \approx I_i(0)\exp(G_0 l) . \quad (6)$$

To generate a field I_i with an energy in the μJ range, the amplification-length product $G_0 l$ has to be about 30 [40]. In a corresponding energy equation to (6), $E_i(0)$ is the energy of one photon at a fixed wavelength. At the center wavelength of the visible continuum (760 nm) the effective amplification length was determined above by the walk-off angle to about 1.2 mm, yielding then an amplification coefficient G_0 of 250 $\rm cm^{-1}$. Such a high amplification coefficient is also obtained from formula (5) using calculated and measured $\chi^{(3)}$ values as discussed below.

At high amplifications, a difference-frequency-mixing process, self-starting from quantum noise, is possible as has been observed in Ref. [21]. Here, in addition, start photons at $\omega_{\rm vis}$ and $\omega_{\rm vuv}$ may also be generated by amplified spontaneous emission and near resonant hyper-Raman scattering in the xenon molecules. The xenon molecules concentration at room temperature amounts to 0.5% of the atomic density [41]. In our experiments at a pressure of 30 Torr this corresponds to a molecule density of about 10^{15} $\rm cm^{-3}$. By two-photon excitation of the xenon dimer ground state—bounded by van der Waals interactions—energetically high-lying molecular states, corresponding to the atomic $6p$ states at large internuclear distances, can be populated, allowing spontaneous, stimulated, and hyper-Raman laser-type transitions to the excited molecular 0^+ states [42] (see also Fig. 1). Photons generated by such processes fit to the visible spectral range (650–850 nm), and could serve as start photons, and may also be responsible for the observed transversal continuum [Fig. 9(c)] and the weak coaxial continuum emitted antiparallel to the pump laser [Fig. 9(b)]. Due to the population of the 0^+ levels and reabsorption of the vuv emission around 147 nm, vuv fluorescence around 148 and 165 nm is also obtained, as can be seen in the transversal spectrum [Fig. 14(b)], corresponding to transitions into the repulsive or weakly bound 0_g^+ state. These transitions are well known as the I and II continua in a xenon discharge [43]. Generated photons in the wavelength range between 650 and 850 nm interact with the pump-laser photons, are amplified, and generate the corresponding vuv photons, if the phase-matching condition is accomplished. The generation of the photons in the small signal gain approximation

occurs exponentially according to Eq. (4) or (6). At macroscopic intensities for ω_{vis} and ω_{vuv} this FWPO process is superimposed by FWM, as is well known from experiments, where three photons are irradiated, generating a fourth photon. In these parametric mixing processes also a cascading spectral broadening is involved, leading to the observed spectra.

The vuv radiation generated around 150 nm can be absorbed in the molecular xenon [41]. Therefore the xenon density and with it the density of the xenon molecules has to be limited to values around 10^{17} cm^{-3}, as has been determined by absorption measurements of the generated vuv emission in an additional xenon cell, operating at different pressures. This absorption also explains the relatively low optimum densities compared to normal mixing schemes and the lower conversion efficiency of 0.6% in the vuv, compared to the corresponding efficiency of 1.2% in the visible spectral range.

2. *uv emission*

At higher xenon pressures a further strong continuum emission in the uv spectral range between 185 and 400 nm has been observed parallel to the pump-laser direction (Fig. 18). In the presented spectrum the short-wavelength spectral range around the pump-laser wavelength (λ=248.5 nm) and below is cut off by dielectric filters. For the remaining spectral range (λ=270–400 nm) output energies of more than 70 μJ have been measured at xenon pressures of 700 Torr and a pump-laser energy of 5.5 mJ. For the whole uv spectral range between 185 and 400 nm a total output energy of more than 150 μJ is estimated. By an autocorrelator based on two-photon ionization of trimethylamine (TME) (TME-ionization potential: 7.82 eV [37], TME pressure: 10 Torr) the pulse duration at 300 nm has been determined to about 360 fs, thus corresponding to the pump pulse duration. For this uv emission also a conical emission profile is observed, indicating again a parametric difference frequency mixing process as in the visible-vuv spectral range, which is noncollinear phase matched. The observed opening angles, however, are small compared to the cones in the visible spectral range. Again, we assume for this strong uv emission a four-wave parametric-oscillation process, according to $2\omega_p = \omega_{uv}^{*} + \omega_{uv}^{**}$ with ω_{uv}^{*} and ω_{uv}^{**} being corresponding frequencies in the uv spectral range. The start photons for this FWPO scheme must be generated purely by parametric fluorescence, due to large energy detuning ($\Delta E > 5000$ cm^{-1}) of the generated wavelengths from any relevant atomic and molecular resonances. For an average walk-off length of 12 mm at the 280-nm center wavelength (p=560 Torr), the observed output energies correspond in the small signal gain approximation—according to Eq. (5)—to a gain coefficient G_0 of more than 30 cm^{-1}.

Comparable high amplification factors as obtained here for both FWPO processes, to our knowledge, have so far only been observed in near-resonant parametric four-wave-mixing schemes at detunings smaller than 10 cm^{-1}, where the nonlinear susceptibility $\chi^{(3)}$, which determines G_0, is resonantly enhanced. Taking our experimental data, we determined some values of the nonlinear susceptibility in xenon for four-wave frequency mixing processes by application of Eq. (5). The effective amplification length l is determined by the walk-off length and the number density N is given by the experimental values. For the pump-laser intensity I_p an average value of 10^{14} W/cm^2 has been assumed. In the uv spectral range at 280 nm, where also the absorption of the generated radiation in xenon can be neglected, the microscopic susceptibility amounts to $|\chi^{(3)}(280\text{ nm})| = 5\times10^{-51}$ m^5/V^2. Taking into account an absorption coefficient of 0.08 cm^{-1} [41] at the center wavelength of 148.5 nm in the vuv spectral range, a value of $|\chi^{(3)}(148.5\text{ nm})| = 10^{-48}$ m^5/V^2 can be determined, which is enhanced compared to the susceptibility in the uv by the $6s[\frac{3}{2}]_1^{\circ} \rightarrow 5p^6\,{}^1S_0$ xenon resonance line at 146.9 nm. These values agree well with susceptibility values determined from difference-frequency-mixing experiments as mentioned below, where in addition to the pump field at ω_p a macroscopic field at either ω_{vis} or ω_{uv} was irradiated into the xenon cell [44]. A comparison of these experimental values with theoretical values of $|\chi^{(3)}|$ calculated for a fixed pump-laser detuning of 0.2 nm from the $6p[\frac{1}{2}]_0$ two-photon resonance is shown in Fig. 19 for the spectral range between 130 and

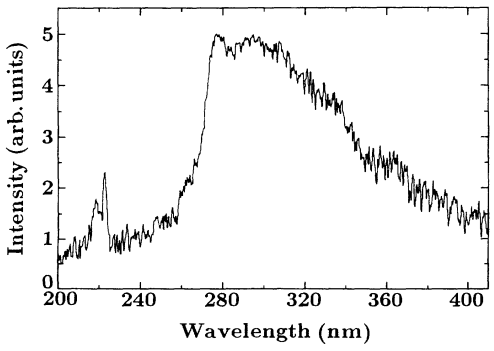

FIG. 18. Forward emission spectrum of the coherent uv continuum radiation for a xenon pressure of 400 Torr and a pump-laser energy of 5 mJ.

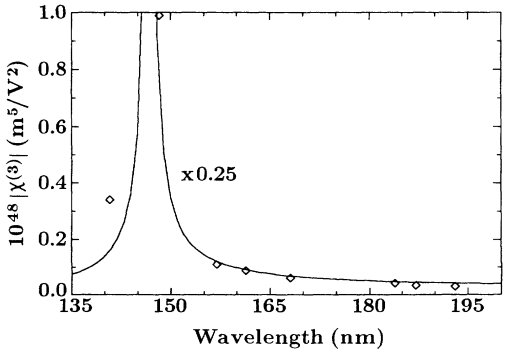

FIG. 19. Calculated spectral dependence of the nonlinear susceptibility $|\chi^{(3)}|$ of xenon for the conversion process $\omega_{vuv} = 2\omega_p - \omega_{vis}$. Experimentally determined values are indicated by rhombs.

200 nm. For the calculations a four-level system has to be assumed including the $6s[\frac{3}{2}]_1^\circ$, $6s'[\frac{1}{2}]_1^\circ$, $6p[\frac{1}{2}]_0$, and $5p^6$ state [40]. Necessary atomic data such as oscillator strengths have been taken from Ref. [31]. Saturation and transient effects, damping rates, and also the level shift by the ponderomotive potential have not been included in the calculation. From Fig. 19 it can be seen that the nonlinear susceptibilities achieve maximum values around 148 nm, where in the experiments the highest amplification factors for the FWPO process have been found.

IV. CONCLUSIONS

The experiments performed on two-photon excitation of xenon with intense femtosecond KrF-excimer-laser pulses have led to the observation of a number of coupled nonlinear processes, with additional features. These concern especially an influence of ponderomotive level shifts in connection with the observed infrared line radiation and the broadband and intense emission in the visible, uv, and vuv spectral range. The emission of these continua, with a spectral width of more than 4000 cm^{-1} and pulse energies up to 100 μJ, can be explained by noncollinear phase-matched self-starting four-wave-mixing processes. Calculated and measured gain coefficients are in good agreement and consistent with a generation process starting from quantum noise. Whether other processes, such as spontaneous or stimulated hyper-Raman-type emissions from xenon molecules, also contribute to a start field has to be investigated further. Also the role of the ponderomotive potential and the coupling of ASE and hyper-Raman processes for the infrared line emission need more detailed studies.

Furthermore, the response time of the xenon atoms in the interaction process has to be examined in additional experiments to determine transient characteristics of the nonlinear susceptibility, as so far all considerations and calculations are based on a stationary susceptibility formalism.

The emissions obtained from the xenon cell can immediately be applied for spectroscopic purposes and the underlying four-wave-mixing scheme can now also be used to generate powerful tunable ultrashort radiation by use of additional pump-laser fields. For example, by spectral filtering of the continuum emissions, tunable short pulse radiation with μJ energies in the ranges of 650–800 and 250–400 nm can be obtained for applications or for further amplification. If an additional pump field is injected into the xenon cell, ordinary four-wave mixing is possible. In this way by injection of suitable nanosecond pump-laser radiation in the visible or uv spectral range, fs pulses at μJ energies have been generated at various wavelengths in the range 132–355 nm. At wavelengths of 351, 308 and 193 nm the radiation has been further amplified in the corresponding excimer-laser amplifier (XeF, XeCl, and ArF, respectively) to short pulse radiation at mJ output energies [44].

The described processes are of course not limited to xenon. Using other atoms such as krypton and mercury or even molecules such as carbon monoxide and hydrogen and appropriate pump-laser sources, comparable two-photon excited FWPO and FWM schemes should be possible, with the potential to generate even much shorter wavelength fs pulses. In the case of krypton, near-resonant two-photon excitation at wavelengths of 216 (second-order stimulated anti-Stokes Raman scattering from 248 nm in H_2) or 193 nm is possible, with the option to produce powerful coherent short pulse radiation at hydrogen Lyman α (121.6 nm). In some initial experiments on mercury with two-photon excitation by the femtosecond KrF-laser coherent short pulse radiation at $\lambda = 122$, 125, and 130 nm with output energies in the μJ range have already been obtained [45].

[1] S. L. Chin and P. Lambropoulos, *Multiphoton Ionization* (Academic, London, 1984).

[2] M. H. Mittleman, *Theory of Laser-Atom Interaction* (Plenum, London, 1982).

[3] Y. R. Shen, *Nonlinear Infrared Generation* (Springer-Verlag, Berlin, 1977).

[4] M. Dörr, R. M. Potvliege, and R. Shakeshaft, Phys. Rev. A **41**, 558 (1990).

[5] H. G. Muller, H. B. van Linden van der Heuvell, P. Agostini, G. Petite, A. Antonetti, M. Franco, and A. Migus, Phys. Rev. Lett. **60**, 565 (1988).

[6] A. McPherson, G. Gibson, H. Jara, U. Johann, T. S. Luk, I. A. McIntyre, K. Boyer, and C. K. Rhodes, J. Opt. Soc. Am. B **4**, 595 (1987).

[7] S. E. Harris, Phys. Rev. Lett. **31**, 341 (1973).

[8] A. Tünnermann, R. Henking, and B. Wellegehausen, Appl. Phys. Lett. **58**, 1004 (1991).

[9] J. F. Reintjes, *Nonlinar Optics Parametric Processes in Liquids and Gases* (Academic, London, 1984).

[10] C. R. Vidal, in *Tunable Lasers,* edited by L. F. Mollenauer and J. C. White, Topics in Applied Physics Vol. 59 (Springer-Verlag, Berlin, 1987).

[11] R. T. Hodgson, P. Sorokin, and J. J. Waynne, Phys. Rev. Lett. **32**, 343 (1974).

[12] R. Hilbig and R. Wallenstein, IEEE J. Quantum Electron. **QE-19**, 1759 (1983).

[13] S. M. Hamadani, J. A. Stockdale, R. N. Compton, and M. S. Pindzola, Phys. Rev. A **34**, 1938 (1986).

[14] R. Hilbig and R. Wallenstein, IEEE J. Quantum Electron. **QE-19**, 194 (1983).

[15] G. Hilber, A. Lago, and R. Wallenstein, J. Opt. Soc. Am. B **4**, 1753 (1987).

[16] J. P. Marangos, N. Shen, H. Ma, H. R. Hutchinson, and J. P. Connerade, J. Opt. Soc. Am. B **7**, 1254 (1990).

[17] F. Vallee and J. Lukasik, Opt. Commun. **43**, 287 (1982).

[18] U. Czarnetzki and H. F. Döbele, Phys. Rev. A **44**, 7530 (1991).

[19] R. W. Boyd, Michelle S. Malcuit, D. J. Gauthier, and K. Rzazewski, Phys. Rev. A **35**, 1648 (1987).

[20] M. A. Moore, W. R. Garrett, and M. G. Payne, Phys. Rev. A **39**, 3692 (1989).

[21] R. K. Wunderlich, W. R. Garrett, R. C. Hart, M. A.

Moore, and M. G. Payne, Phys. Rev. A **41**, 6345 (1990).
[22] Y. R. Shen, *The Principles of Nonlinear Optics* (Wiley, New York, 1984).
[23] P. G. Harper and B. S. Wherrett, *Nonlinear Optics* (Academic, London, 1977).
[24] Charlotte E. Moore, in *Atomic Energy Levels,* Natl. Bur. Stand. (U.S.) (U.S. GPO, Washington, DC, 1971).
[25] Marie-Claude Castex, Chem. Phys. **5**, 448 (1974).
[26] A. Tünnermann, K. Mossavi, and B. Wellegehausen, Inst. Phys. Conf. Ser. **126**, Sec. II, 139 (1992).
[27] R. R. Alfano, *The Supercontinuum Laser Source* (Springer-Verlag, Berlin, 1989).
[28] S. Szatmari and F. P. Schäfer, Opt. Commun. **68**, 196 (1988).
[29] N. Morita and Y. Yajima, Appl. Phys. B **28**, 25 (1982).
[30] A. Tünnermann, H. Eichmann, R. Henking, K. Mossavi, and B. Wellegehausen, Opt. Lett. **16**, 402 (1991).
[31] M. Aymar and M. Coulombe, At. Data Nucl. Data Tables **21**, 537 (1978).
[32] D. Kligler, D. Pritchard, W. K. Bischel, and C. K. Rhodes, J. Appl. Phys. **49**, 2219 (1978).
[33] W. R. Garrett, R. C. Hart, J. C. Miller, M. G. Payne, and J. E. Wray, Opt. Commun. **86**, 205 (1991).
[34] L. Pan, L. Armstrong, Jr., and J. Eberly, J. Opt. Soc. Am. B **3**, 1319 (1986).
[35] P. H. Buchsbaum, R. R. Freeman, M. Bashkansky, and T. J. McIlrath, J. Opt. Soc. Am. B **4**, 760 (1987).
[36] J. P. Davis and E. Dressler, Phys. Rev. A **45**, 3104 (1992).
[37] J. A. R. Samson, *Techniques of Vacuum Ultraviolet Spectroscopy* (Wiley, New York, 1967).
[38] A. Bideau-Mehu, Y. Guern, R. Abjean, and A. Johannin-Gilles, J. Quant. Spectrosc. Radiat. Transfer **25**, 395 (1981).
[39] R. Mahon, T. J. McIlrath, V. P. Myerscough, and D. W. Koopman, IEEE J. Quantum. Electron. **QE-5**, 444 (1979).
[40] D. C. Hanna, M. A. Yuratich, and D. Cotter, *Nonlinear Optics of Free Atoms and Molecules* (Springer-Verlag, Berlin, 1979).
[41] Marie-Claude Castex, J. Chem. Phys. **74**, 759 (1981).
[42] M. H. R. Hutchinson, I. A. McIntyre, G. N. Gibson, and C. K. Rhodes, Opt. Lett. **12**, 102 (1987).
[43] Y. Tanaka, J. Opt. Soc. Am. **45**, 710 (1955).
[44] A. Tünnermann, C. Momma, K. Mossavi, C. Windolph, and B. Wellegehausen, IEEE J. Quantum. Opt. (to be published).
[45] C. Momma, A. Tünnermann, L. Pfitzner, and B. Wellegehausen (unpublished).

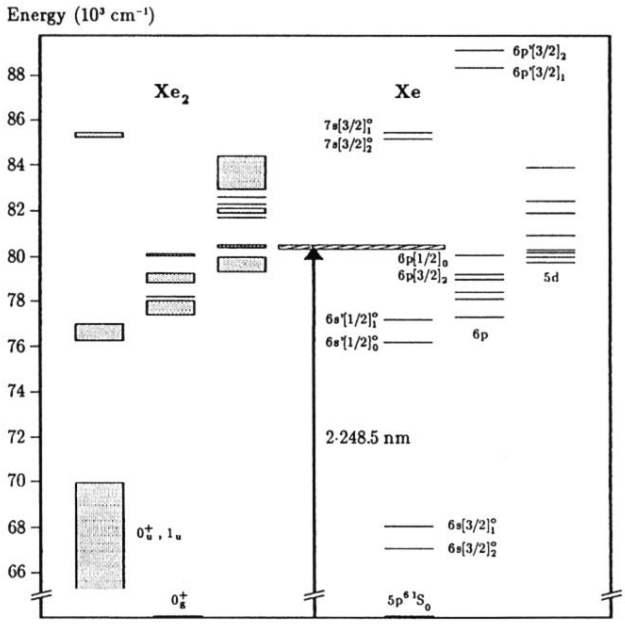

FIG. 1. Relevant energy-level diagram of atomic and molecular xenon. Molecular absorption bands are indicated by the hatched areas (after Refs. [24,25]).

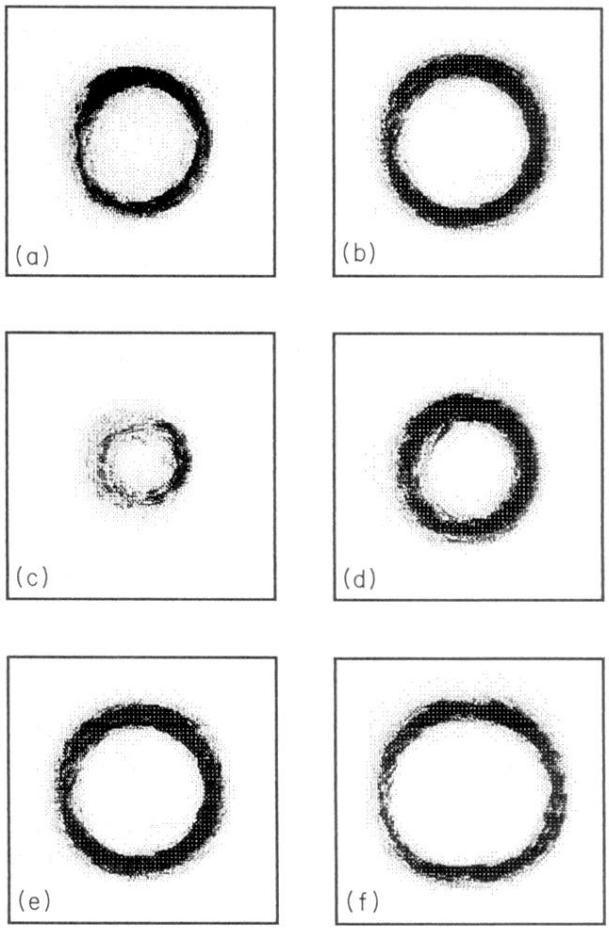

FIG. 13. Conical emission profiles of the visible radiation (forward direction) (a) $\lambda = 670$ nm; (b) $\lambda = 760$ nm; (c)–(f) increasing xenon pressure ($\lambda = 760$ nm).